Journal of Molecular Graphics and Modelling 34 (2012) 10–17

Contents lists available at SciVerse ScienceDirect

Journal of Molecular Graphics and Modelling

journal homepage: www.elsevier.com/locate/JMGM

Probing the simulant behavior of PNPDPP toward parathion and paraoxon: A computational study

Md Abdul Shafeeuulla Khan[a], Tusar Bandyopadhyay[b], Bishwajit Ganguly[a,*]

[a] Analytical Science Discipline, Central Salt & Marine Chemicals Research Institute (Council of Scientific and Industrial Research), Bhavnagar, Gujarat 364002, India
[b] Theoretical Chemistry Section, Chemistry Group, Bhabha Atomic Research Centre, Trombay, Mumbai 400085, India

ARTICLE INFO

Article history:
Received 17 May 2011
Received in revised form
22 December 2011
Accepted 26 December 2011
Available online 31 December 2011

Keywords:
Alkaline hydrolysis
Paraoxon
Parathion
PNPDPP
Simulant

ABSTRACT

The extreme toxicity of organophosphorus nerve agents and pesticides mandates to employ models or simulants in place of the actual compounds in the laboratory. The importance of simulants is known, however, their efficacy for direct comparison with the toxic organophosphorus compounds is not well documented. We have examined the potential energy surfaces (PES) for the alkaline hydrolysis of pesticides like paraoxon (diethyl 4-nitrophenyl phosphate), parathion (O,O-diethyl O-4-nitrophenyl phosphorothioate) and PNPDPP (4-nitrophenyl diphenyl phosphate), a simulant with MP2/6-311 + G*//B3LYP/6-311 + G* + ΔG_{solv} (HF/6-31 + G*) level of theory. The effect of aqueous solvation was considered with the Integral Equation Formalism Polarizable Continuum Model (IEF-PCM). The alkaline hydrolysis of these organophosphorus compounds reveals that the reaction proceeds through the attack of hydroxide ion at the phosphorus center to form a pentacoordinate intermediate. The calculated free energies of activation for the alkaline hydrolysis of paraoxon and parathion are in good agreement with the available experimental activation free energies. The computed results show that the reaction profiles for the alkaline hydrolysis of paraoxon, parathion and PNPDPP are largely similar; however, the rate of hydrolysis of parathion may be higher than that of paraxon and PNPDPP. Such difference arises due to the less electrophilic nature of the phosphorus atom of parathion molecule as observed in the charge analysis study. The conceptual DFT analysis also showed the similar trend for the alkaline hydrolysis of paraoxon, parathion and PNPDPP with hydroxide anion. This computational study provides a quantitative support toward the use of PNPDPP as a simulant for organophosphorus compounds, which cannot be used directly for the laboratory purposes.

1. Introduction

Several persistent chemicals such as paraoxon, parathion and chemical warfare compounds such as VX, sarin etc. are hydrophobic phosphorus (V) esters or phosphylating agents [1]. They can irreversibly react with the enzyme acetylcholinesterase (AChE), inhibiting its control over the central nervous system [1–3]. AChE catalyzes the ester hydrolysis of the neurotransmitter acetylcholine (ACh) to terminate synaptic transmission [4–6]. Inhibition of AChE occurs as a result of the phosphylation of the active serine residue with organophosphorus (OP) compounds [7–9]. Such AChE inhibition results in acetylcholine accumulation at cholinergic receptor sites, thereby excessively stimulating the cholinergic receptors. This can lead to various clinical disorders sometimes causes death. Remediation of such toxic contaminants therefore continues to be a challenge for research groups. In particular, chemical means of achieving efficient destruction of organophosphorus esters remains an active area of research. The easy hydrolysis of these toxic organophosphorus esters is one of the prime focuses in recent times [10,11]. Other detoxification methods have also been explored using oxidizing agents, photocatalysis, metal-catalyzed decomposition, enzyme degradation, and reduction [12–17].

Paraoxon and parathion are the compounds most often responsible for the poisoning of agricultural workers [18]. The extreme toxicity of these nerve agents mandates that most laboratory research utilizes models or simulants in place of these hazardous compounds [10,19]. Especially, many researchers use PNPDPP as a simulant to develop effective decontaminating reagents toward actual compounds [20–24]. PNPDPP has become the unauthorized standard simulant for phosphotriester hydrolytic reactions, since its introduction in 1969 [24]. Use of simulant allows ready comparison of kinetic data obtained with many different nucleophiles under varying reaction conditions due to its non-toxicity and the structural similarity with many organophosphorus (OP) compounds [21]. However, the literature lacks the comparative

* Corresponding author. Fax: +91 278 2567562.
E-mail address: ganguly@csmcri.org (B. Ganguly).

1093-3263/$ – see front matter © 2012 Elsevier Inc. All rights reserved.
doi:10.1016/j.jmgm.2011.12.008

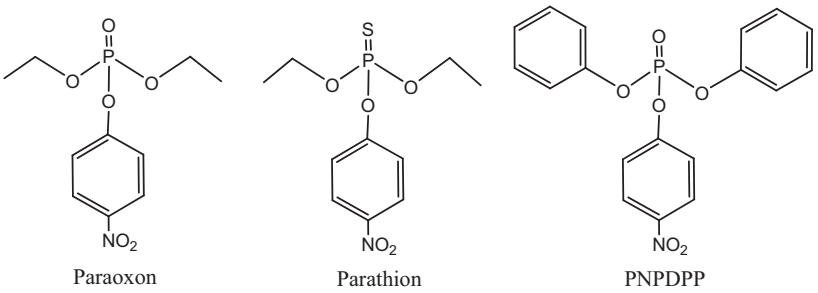

Scheme 1. Structures of organophosphorus compounds paraoxon, parathion and PNPDPP (simulant).

data for PNPDPP and other OP compounds to validate the use of former compound as simulant. This prompted us to examine the simulant behavior of PNPDPP toward paraoxon and parathion by exploring the alkaline hydrolysis of these compounds (Scheme 1). Generally, the selection of appropriate simulants for the hydrolysis will depend primarily on the presence of the bonds in the simulant compounds at which the hydrolysis reaction occurs in the original compounds. The best simulant will closely match the structure of the original compound and can potentially form the same or similar hydrolysis products [25]. The alkaline hydrolysis process of paraoxon, parathion and PNPDPP has been studied employing density functional theory (DFT) and Møller–Plesset (MP2) calculations. Further the reactivity trends have been examined with the conceptual DFT analysis.

2. Computational methodology

A thorough conformational search was performed with the Macromodel program using MMFFs force field for paraoxon, parathion and PNPDPP [26–30]. Conformational search was performed with the random variation of all the rotatable bonds and combining the Monte Carlo conformational search (MCMM) algorithm [31,32] using 5000 Monte Carlo steps. Energy minimizations were performed with the Polak–Ribiere conjugate gradient (PRCG) method [33], which involves the use of first derivatives with the default convergence criterion 0.05 kJ/mol Å. Sorted all found conformations according to energy. Conformations whose relative energy was within 50 kJ/mol with respect to lowest energy structure were stored. The ensuing conformations were clustered based on torsional RMS using XCluster approach [34,35]. Based on the minimum separation ratio, two representative conformations in each case were chosen from this clusterization procedure. The selected conformations from the conformational families were stored for further higher level DFT calculations. The lowest energy conformations obtained at DFT calculations were considered to model the alkaline hydrolysis process. We have modeled the alkaline hydrolysis process by employing MP2/6-311 + G*//B3LYP/6-311 + G* + ΔG_{solv} (HF/6-31 + G*) composite level of theory which was chosen based on the bench marking of methods (please see Section 3).

All geometries involved in the alkaline hydrolysis processes were optimized using the B3LYP [36–38] density functional and the 6-311 + G* basis set. Harmonic frequency calculations at the same level were used to validate the stationary points and to estimate thermodynamic corrections. Intrinsic reaction coordinate (IRC) calculations were performed to connect all the transition states with their corresponding minima [39,40]. Single-point electronic energies were obtained at the MP2/6-311 + G* [41,42] level of theory. Free energies of solvation in water were determined at the HF/6-31 + G* level of theory using the Integral Equation Formalism Polarizable Continuum Model (IEF-PCM) [43] along with the UFF topological model [44], which places an explicit sphere on every atom. Energies reported in this study are free energies obtained from normal mode analysis with the harmonic approximation and no statistical simulations were carried out. All quantum chemical calculations were performed using Gaussian 03, Revision E.01 and Gaussian 09, Revision B.01 programs [45].

For conceptual DFT calculations, the local softness $s(r)$ can be obtained as

$$s(r) = f(r)S \tag{1}$$

where S is the global softness of the species and $f(r)$ is the so-called Fukui function [46]. Within a finite difference approximation, combined with the idea of integrating the Fukui function over atomic regions, one finds the condensed Fukui functions for nucleophilic and electrophilic attack on atom A having N electrons with Eqs. (2) and (3), respectively.

$$f_A^+ = q_A(N_0 + 1) - q_A(N_0) \tag{2}$$

$$f_A^- = q_A(N_0) - q_A(N_0 - 1) \tag{3}$$

where $q_A(N_0)$, $q_A(N_0 + 1)$, and $q_A(N_0 - 1)$ are the atomic populations for atom A in the neutral molecule and its corresponding anion and cation, respectively. For calculating the condensed Fukui function f_A, natural population charge analysis (NPA) [47] was performed on optimized geometries of OH^- and OP compounds at the recommended B3LYP/6-31 + G(d,p) level of theory [36,48]. The global softness S is given by the finite difference approximation.

$$S = \frac{1}{I - A} \tag{4}$$

where I and A represents the ionization energy and the electron affinity, respectively. For calculating global softness, one can apply Koopmans' theorem [49] (assumption of frozen orbitals), approximating I by the energy of the highest occupied molecular orbital (ε_{HOMO}) and A by the energy of the lowest unoccupied molecular orbital (ε_{LUMO}).

$$S = \frac{1}{\varepsilon_{LUMO} - \varepsilon_{HOMO}} \tag{5}$$

Further, the local softness for nucleophile and electrophile can be calculated with Eqs. (6) and (7), respectively.

$$s_A^+ = Sf_A^+ \tag{6}$$

$$s_A^- = Sf_A^- \tag{7}$$

In the present study, s^+ indicates the local softness of oxygen of nucleophiles and s^- the local softness of phosphorus of sarin.

According to HSAB principle and in analogy with earlier work by Gázquez [50] and Geerlings et al. [51] and its generalization by Ponti [52], the preferred reactivity between the reaction partners can be based on the difference in local softness $s(r)$ of the interacting parts (atoms, functional groups) of these reaction partners should be minimal for most favorable interactions.

$$\Delta s(r) = |s^+(r) - s^-(r)| \tag{8}$$

Table 1
Computed activation free energies for alkaline hydrolysis of organophosphorus compounds paraoxon and parathion using different methods.

Method	Paraoxon[c]	Parathion[c]
B3LYP/6-31 + G*//B3LYP/6-31 + G*[a]	17.3	18.5
MP2/6-31 + G*//B3LYP/6-31 + G*[a]	16.8	18.1
MP2/6-31 + G*//B3LYP/6-31 + G*[b]	22.5	24.3
B3LYP/6-311 + G*//B3LYP/6-311 + G*[a]	16.3	17.6
MP2/6-311 + G*//B3LYP/6-311 + G*[a]	15.9	17.1
MP2/6-311 + G*//B3LYP/6-311 + G*[b]	21.8	22.9

[a] Singlepoint calculations were performed in aqueous phase.
[b] Single point calculations were performed in gas phase and the solvation was accounted with correction of ΔG_{solv} obtained at HF/6-31 + G* level.
[c] Reported [56] experimental activation free energy of paraoxon is 20.0 ± 0.3 and that of parathion is 21.5 ± 0.2.

3. Results and discussion

To find an accurate method that is computationally efficient, calculations were performed at various levels of theories for the alkaline hydrolysis of paraoxon and parathion whose experimental results are available in the literature. Free energies of activation for the alkaline hydrolysis of these two compounds were computed using the popular hybrid DFT method B3LYP. Second-order Møller–Plesset theory (MP2) was also used for the same purpose because DFT has been known to underestimate the barrier heights [53,54]. Two basis sets were used in conjunction with the methods mentioned above: 6-31 + G* and 6-311 + G*.

We have optimized all geometries at two different levels viz. B3LYP/6-31 + G* and B3LYP/6-311 + G*. The single point B3LYP and MP2 calculations in aqueous phase using two basis sets 6-31 + G* and 6-311 + G* on B3LYP/6-31 + G* and B3LYP/6-311 + G* gas phase optimized geometries computed the activation free energies for the alkaline hydrolysis of paraoxon in the range 16.0–17.0 kcal/mol and that of parathion in the range 17.0–18.0 kcal/mol. These results show that the calculated activation free energies are not close to the experimentally determined values [55]. Earlier studies of phosphate ester hydrolysis have shown that the composite level of theory is more accurate to reproduce the experimental results and we have also employed the composite levels here [56]. Therefore, we have examined solvation effect from HF/6-31 + G* (corrected with ΔG_{solv}) on B3LYP/6-31 + G* and B3LYP/6-311 + G* optimized stationary points. Solvation accounted with the correction of ΔG_{solv} (obtained at HF/6-31 + G*) seems to adequately predict the barrier heights as compared to the other solvation effects (Table 1). We compared our computed activation free energies for the alkaline hydrolysis of paraoxon and parathion with the reported experimental activation free energies for the same [55]. The activation free energies obtained at MP2/6-31 + G*//B3LYP/6-31 + G* with the solvation correction from HF/6-31 + G* were found to be 22.5 kcal/mol and 24.3 kcal/mol for the alkaline hydrolysis of paraoxon and parathion respectively. But the activation free energies obtained at MP2/6-311 + G*//B3LYP/6-311 + G* with the solvation correction from HF/6-31 + G* were found to be 21.8 kcal/mol and 22.9 kcal/mol for the alkaline hydrolysis of paraoxon and parathion respectively. The reported experimental activation free energies for the alkaline hydrolysis of paraoxon and parathion are 20.0 ± 0.3 kcal/mol and 21.5 ± 0.2 kcal/mol respectively. The activation free energies for alkaline hydrolysis of paraoxon and parathion obtained at MP2/6-311 + G*//B3LYP/6-311 + G* + ΔG_{solv} (HF/6-31 + G*) level of theory were found to be in close agreement (around ca. ± 1.0 kcal/mol) with the available experimental results as compared to all other levels of theories engaged in this study (Table 1). Therefore, the potential energy surface for the alkaline hydrolysis of PNPDPP has also been computed at MP2/6-311 + G*//B3LYP/6-311 + G* + ΔG_{solv} (HF/6-31 + G*) level of theory.

The hydrolysis of phosphotriesters has been studied earlier because they are classical reactions of fundamental importance in chemistry and biology. In particular, PNPDPP has been extensively used in many studies [21,23,24]. Generally, solvolysis of organophosphorus compounds follows the addition–elimination pathway involving a trigonal bipyramidal (TBP) intermediate [19,57–63]. However, the computational study performed for the alkaline hydrolysis of paraoxon by Zheng et al. showed that the hydrolysis process of paraoxon is a concerted one at MP2/6-31 + G*//HF/6-31 + G* level of theory [19].

To examine the hydrolysis of parathion, paraoxon and PNPDPP, we have initially performed an extensive conformational search due to their structural flexibility. Two unique conformers were identified in each case during the conformational search process using MMFFs force field in aqueous phase (GB/SA) after clusterization of the conformations. These conformers were further optimized at B3LYP/6-311 + G* level of theory and the stable conformers have been considered to model the alkaline hydrolysis process. The reaction energy profiles obtained for the attack of hydroxide anion with parathion, paraoxon and PNPDPP follows the addition–elimination pathway involving a trigonal bipyramidal intermediate.

3.1. Alkaline hydrolysis of paraoxon

The hydrolysis of organophosphorus esters in aqueous solution is viewed that hydrolysis of monoesters proceeds by a dissociative, unimolecular elimination pathway, whereas, the diesters and triesters follow a bimolecular base catalyzed hydrolysis mechanism. Recent studies suggest that reactions of nucleophiles with neutral phosphoryl species could proceeds through a two-step pathway involving a pentacoordinate intermediates [19,57–63]. In general, the most electronegative group thermodynamically prefers the apical position in trigonal bipyramidal phosphorus compounds, and also elimination is more facile from an apical position [58–65]. Thus, the most electronegative group may be expected to be the preferred leaving group in the absence of any other electronic or steric factors. In the case of paraoxon, 4-nitrophenolate is more electronegative compared to that of ethoxide groups, therefore more apicophilic and can be a good leaving group.

The energy profiles for this reaction pathway and its corresponding optimized geometries are given in Figs. 1a and 2 respectively. The anionic nucleophile and paraoxon stabilizes through charge dipole type interactions besides two C—H···O type hydrogen bonds in the **TS1a** (Fig. 2). The free energy of activation computed for the attack of HO^- to the paraoxon is 21.8 kcal/mol. HO^- approaches opposite to the oxygen atom of leaving moiety in a slightly nonlinear fashion (∠O—P—O = 165.6°) and the P···OH bond distance is 3.107 Å (**TS1a**) (Fig. 2). After **TS1a**, TBP intermediate **INa** has been found to be 0.1 kcal/mol stable than the separated reactants. The —P—OH bond distance and the bond distance between P and oxygen atom of leaving group are 1.736 Å and 1.930 Å, respectively in **INa**. In this intermediate, the P—OH bond shortens and P—SR bond lengthens compared to the transition state **TS1a**. The elimination of the leaving 4-nitrophenolate group is exergonic in nature and requires only 0.6 kcal/mol free energy of activation from the intermediate **INa**. In the second transition state **TS2a**, the P—OH bond further shortens to 1.687 Å and P—SR bond lengthens to 2.178 Å (Fig. 2) showing bonding of oxygen with phosphorus and leaving of 4-nitrophenolate group. Finally, the cleavage of —P—OPh bond results in exergonic products diethyl hydrogen phosphate (**P1a**) and 4-nitrophenolate (**P2a**) (Fig. 1a). The solvolysis process between the hydroxide and paraoxon is governed by the first step and the subsequent steps are downhill in nature at MP2/6-311 + G*//B3LYP/6-311 + G* + ΔG_{solv} (HF/6-31 + G*) level of theory. The intrinsic reaction coordinate calculations (IRC) using

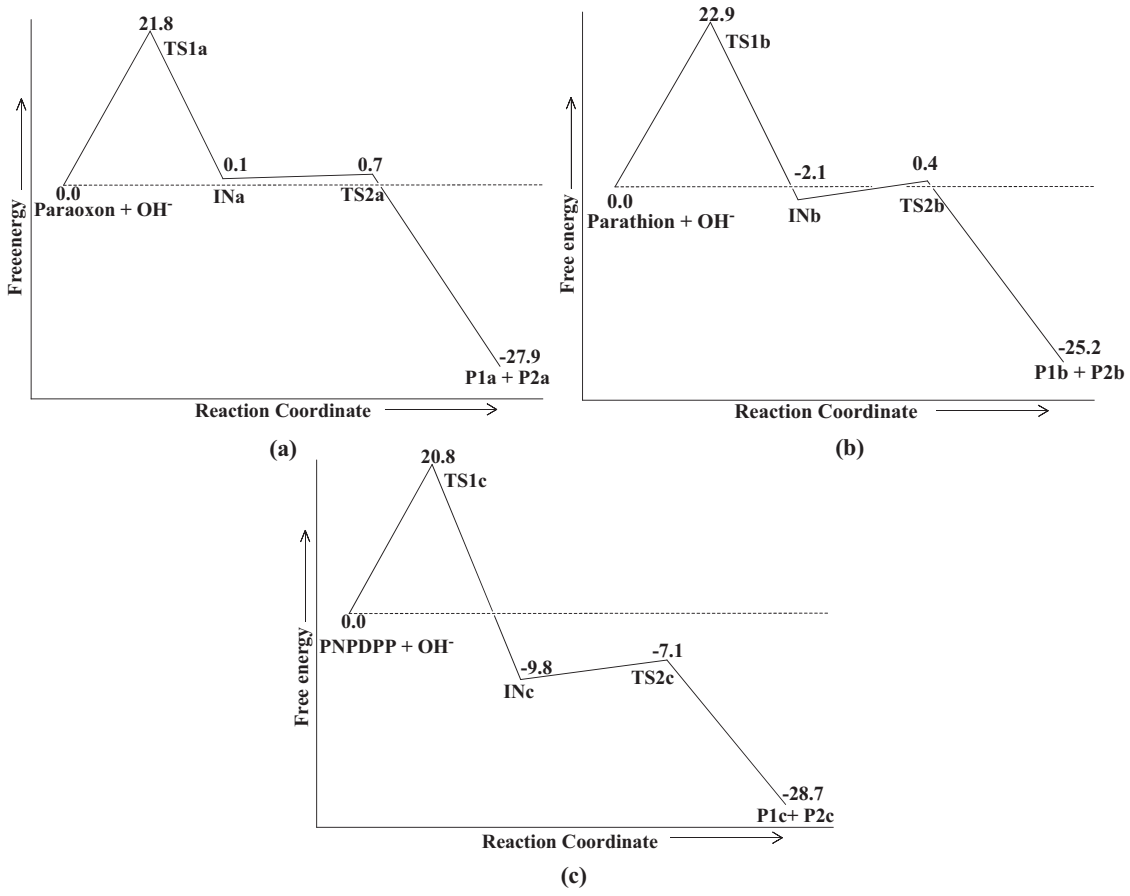

Fig. 1. Potential energy surfaces calculated at MP2/6-311 + G*//B3LYP/6-311 + G* + ΔG_{solv} (HF/6-31 + G*) level of theory for the alkaline hydrolysis of paraoxon (a), parathion (b) and PNPDPP (c).

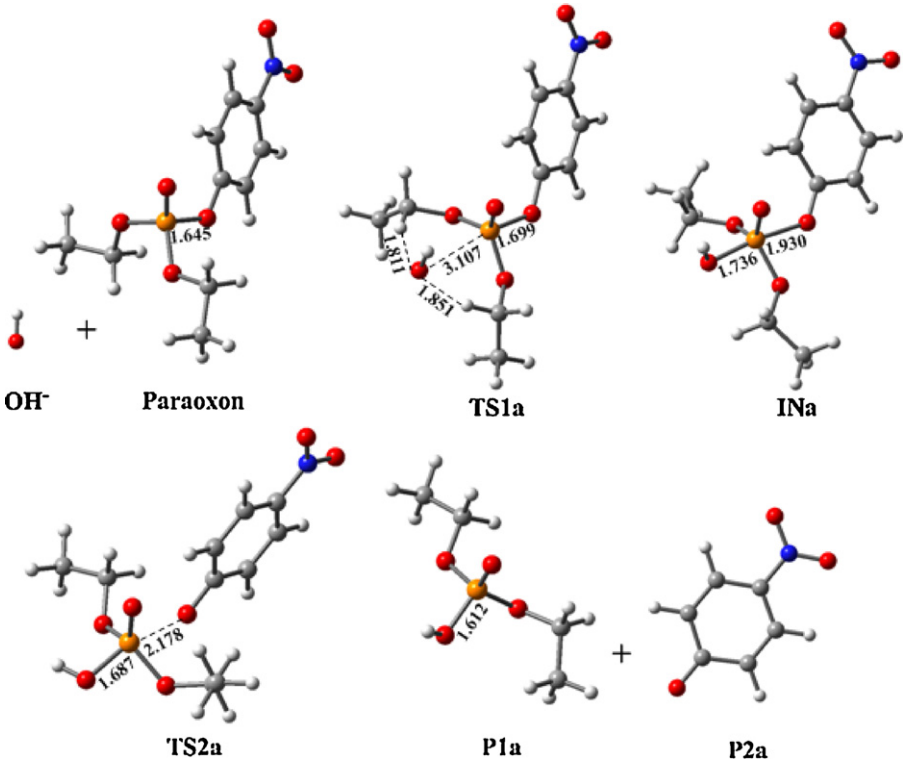

Fig. 2. B3LYP/6-311 + G(d) optimized geometries and selected bond distances (Å) for organophosphorus species involved in the alkaline hydrolysis of paraoxon. (Red = oxygen; orange = phosphorus; gray = carbon; blue = nitrogen; white = hydrogen). (For interpretation of the references to color in figure caption, the reader is referred to the web version of the article.)

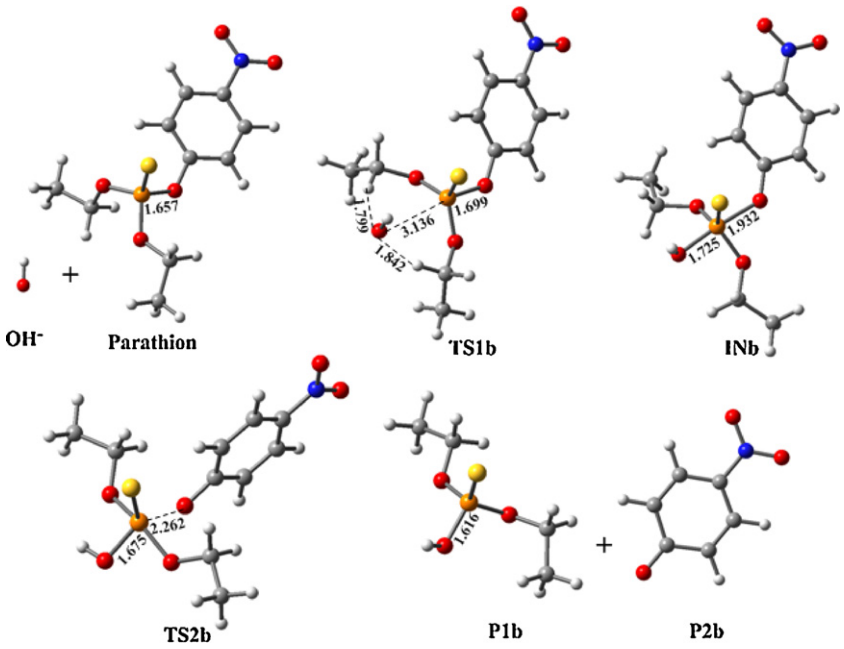

Fig. 3. B3LYP/6-311 + G(d) optimized geometries and selected bond distances (Å) for organophosphorus species involved in the alkaline hydrolysis of parathion. (Red = oxygen; orange = phosphorus; yellow = sulphur; gray = carbon; blue = nitrogen; white = hydrogen). (For interpretation of the references to color in figure caption, the reader is referred to the web version of the article.)

the step size of 50 in units of 0.01 amu$^{1/2}$-Bohr revealed that the transition state **TS1a** in forward direction connects with pentacoordinate intermediate **INa** which supports the mechanism suggested for phosphate diesters and triesters [19]. The alkaline hydrolysis of paraoxon has been reported with activation enthalpy of 9.5 kcal/mol at MP2/6-31 + G*//HF/6-31 + G* level of theory by Zheng et al. [19], which is much lower compared to the experimentally determined activation enthalpy for this reaction [55] and the reaction was found to be concerted rather than two step process. They have also reported that at the Hartree–Fock level, the TBP intermediate and the corresponding second transition state were not obtained.

3.2. Alkaline hydrolysis of parathion

The potential energy surface calculated with MP2/6-311 + G*//B3LYP/6-311 + G* + ΔG_{solv} (HF/6-31 + G*) for the alkaline hydrolysis of parathion is similar to paraoxon (Fig. 1a and b). The separated reactants directly go to the transition state **TS1b** and the activation free energy is found to be 22.9 kcal/mol. The P—O and P—F bond distances in **TS1b** are 3.136 Å and 1.699 Å, respectively (Fig. 3). Trigonal bipyramidal intermediate **INb** was found to be 2.1 kcal/mol lower in energy as compared to separated reactants on the PES. The P—O and P—F bond distances in trigonal bipyramidal intermediate geometry **INb** are 1.725 Å and 1.932 Å, respectively (Fig. 3). Elimination of 4-nitrophenolate ion proceeds through the transition state **TS2b** with a barrier of 2.5 kcal/mol. The transition state geometry **TS2b** shows the expulsion of 4-nitrophenolate ion and directly goes to the final products O,O-diethyl O-hydrogen phosphorothioate (**P1b**) and 4-nitrophenolate (**P2b**) (Figs. 1b and 3). The formation of products is exergonic in nature (Fig. 1b). The reaction of parathion with hydroxide ion is both thermodynamically and kinetically favored. The higher activation barrier for the formation of transition state **TS1b** than that of transition state **TS2b** reveals that the former transition state would govern the rate of hydrolysis of parathion. The higher activation barrier computed for parathion compared to paraoxon is in good agreement with the earlier experimental report on —P═O vs. —P═S compounds [55].

3.3. Alkaline hydrolysis of PNPDPP

Next, the alkaline hydrolysis process was performed with the simulant PNPDPP. The potential energy surface for this reaction is shown in Fig. 1c and the corresponding stationary points are given in Fig. 4. The rate determining transition state (**TS1c**) for HO^- anion attack lie energetically 20.8 kcal/mol above to separated reactants on the PES. The HO^- anion approaches to the reactive center (phosphorus atom) of PNPDPP and the transition state **TS1c** was located at a distance of 3.152 Å. C—H···O type of interactions was observed between the hydrogen atoms of phenyl groups and the oxygen atom hydroxide ion. The TBP intermediate **1Nc** is 9.8 kcal/mol lower to separated reactants. The intermediate **1Nc** proceed to transition state (**TS2c**) for the expulsion of 4-nitrophenolate ion with a barrier of 2.7 kcal/mol and forms individual products. The products formed in the potential energy surface are **P1c** (diphenyl hydrogen phosphate) and **P2c** (4-nitrophenolate), which lies 28.7 kcal/mol below separated reactants (Fig. 1c). It appears that the activation free energy calculated for parathion is higher than paraxon and PNPDPP. The charge analysis performed with the calculated geometries of these parent systems suggest that the phosphorus atom of parathion is less electrophilic toward the incoming nucleophile compared to PNPDPP and paraoxon, hence, the former would be less reactive for alkaline hydrolysis than paraoxon and PNPDPP (Table S1 of the supplimentary data).

The activation free energies for the formation of TBP intermediates alkaline hydrolysis of PNPDPP, paraoxon and parathion were found to be 20.8 kcal/mol, 21.8 kcal/mol and 22.9 kcal/mol respectively. The $\Delta G^{\ddagger}$ values are closer for paraoxon and parathion compared to activation free energies as obserevd in the experimentla results.

The reactivity order of these OP compounds with hydroxide anion was further examined with the help of conceptual density functional theory. In recent years, conceptual DFT offers many concepts to describe the reactivity between reaction partners. Density

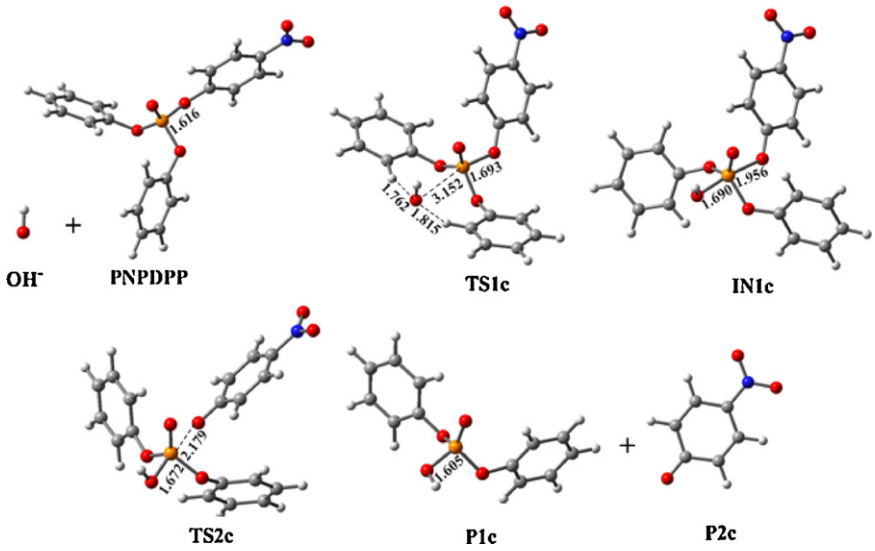

Fig. 4. B3LYP/6-311 + G(d) optimized geometries and selected bond distances (Å) for organophosphorus species involved in the alkaline hydrolysis of PNPDPP. (Red = oxygen; orange = phosphorus; gray = carbon; blue = nitrogen; white = hydrogen.)

Table 2
Global softness (S), local softness (s^+), Fukui function (f^+) and the difference in local softness (Δs) of the OP compounds and OH^- anion calculated at B3LYP/6-31 + G(d,p) in gas phase and aqueous phase ().

Species	Descriptors			
	S	f^+	s^+	Δs
OH^-	3.955	−0.967	−3.824	
	(3.562)	(−0.960)	(−3.421)	–
Paraoxon	5.813	0.002	0.012	3.836
	(6.294)	(0.001)	(0.006)	(3.427)
Parathion	6.432	0.011	0.071	3.895
	(6.435)	(0.007)	(0.045)	(3.466)
PNPDPP	6.309	−0.025	−0.158	3.666
	(6.911)	(−0.024)	(−0.166)	(3.255)

based descriptors have been found to immense usefulness in the prediction of reactivity of atoms and molecules [66,67]. Generally, the advantage of conceptual DFT would be to avoid the non-trivial transition state calculations toward understanding the reactivity of a chemical process in absence of other factors such as steric, thermodynamic and polar factors [68]. Therefore, it is desirable to apply conceptual DFT to explore the reactivity of paraoxon, parathion and PNPDPP of similar geometries toward the alkaline hydrolysis process. The calculations were performed with B3LYP/6-31 + G(d,p) level in gas and aqueous phases for OH^- and OP compounds [40,52]. The computed local softness, global softness and Fukui functions for OH^- and OP compounds are given in Table 2. The reactivity predicted using the difference in local softness (Δs) between OH^- and OP compounds suggests that the alkaline hydrolysis process should follow the order: PNPDPP > paraoxon > parathion (Table 2). The conceptual DFT analyses showed the similar reactivity trend of these OP compounds toward OH^- as observed from the DFT calculations. These results infer that the conceptual DFT methods can be employed to examine the reactivity processes in such compounds [62].

4. Conclusions

In the present study, we have performed *ab initio* molecular orbital and density functional calculations on the alkaline hydrolysis of pesticides like paraoxon, parathion and PNPDPP (*simulant*). The calculated free energies of activation at MP2/6-311 + G*//B3LYP/6-311 + G* + ΔG_{solv} (HF/6-31 + G*) level of theory for the alkaline hydrolysis of paraoxon and parathion were found be in good agreement with the experimental free energies of activation. The DFT results suggest that the hydrolysis of paraoxon, parathion and PNPDPP proceeds through a similar pathway involving the two step addition–elimination mechanisms via the trigonal bipyramidal intermediates. PNPDPP is relatively easier to hydrolyze compared to paraoxon and parathion compounds. The conceptual DFT analysis also supported the faster hydrolysis of the simulant PNPDPP. The slower rate of hydrolysis of parathion compared to paraoxon was also predicted by the DFT conceptual calculations, which is in agreement with the previous report. The overall calculated results suggest that PNPDPP can act as a *simulant* for the pesticides like paraoxon and parathion to avoid their expose in the laboratories, however, cautioned that the relative rates may vary for these compounds, which could be crucial in some cases with new nucleophiles for true comparisons.

Acknowledgments

Authors thank DAE–BRNS, Mumbai, and DST, New Delhi, India for financial support of this work. One of the authors MASK is thankful to DAE-BRNS, India for awarding senior research fellowship. We thank the reviewers for their comments and suggestions, which have helped us to improve the paper.

Appendix A. Supplementary data

Supplementary data associated with this article can be found, in the online version, at doi:10.1016/j.jmgm.2011.12.008.

References

[1] C.A. Buntun, Chemical warfare in Macmillan encyclopedia of chemistry, in: J.J. Lagowsky (Ed.), Macmillan Reference USA, vol. 1, Simon and Schuster Macmillan, New York, 1997, pp. 343–346.
[2] J.J. DeFrank, Organophosphorus cholinesterase inhibitors: detoxification by microbial enzymes, in: J.W. Kelly, T.O. Baldwin (Eds.), Applications of Enzyme Biotechnology, Plenum Press, New York, 1991, pp. 165–180.
[3] E. Heilbronn-Wikstrom, Phosphorylated cholinesterase: their formation reactions and hydrolysis, Sven. Kem. Tidskr. 77 (1965) 598–631.

[4] H.C. Kolb, K.B. Sharpless, The growing impact of click chemistry on drug discovery, Drug Discov. Today 8 (2003) 1128–1137.
[5] D.M. Quinn, Acetylcholinesterase: enzyme structure, reaction dynamics and virtual transition states, Chem. Rev. 87 (1987) 955–979.
[6] A. Shafferman, C. Kronman, Y. Flashner, M. Leitner, H. Grosfeld, A. Ordentlich, Y. Gozes, S. Cohen, N. Ariel, D. Barak, M. Harel, I. Silman, J.L. Sussman, B. Velan, Mutagenesis of human acetylcholinesterase identification of residues involved in catalytic activity and in polypeptide folding, J. Biol. Chem. 267 (1992) 17640–17648.
[7] J. Wang, S. Roszak, J. Gu, J. Leszczynski, Comprehensive global energy minimum modeling of the sarin–serine adduct, J. Phys. Chem. B 109 (2005) 1006–1014.
[8] J. Wang, J. Gu, J. Leszczynski, Phosphonylation mechanisms of sarin and acetylcholinesterase: a model DFT study, J. Phys. Chem. B 110 (2006) 7567–7573.
[9] P. Taylor, S. Lappi, Interaction of fluorescence probes with acetylcholinesterase site and specificity of propidium binding, Biochemistry 14 (1975) 1989–1997.
[10] P.V. Kumar, B. Ganguly, S. Bhattacharya, Computational study on hydroxybenzotriazoles as reagents for ester hydrolysis, J. Org. Chem. 69 (2004) 8634–8642.
[11] E. Gershonov, I. Columbus, Y. Zafrani, Facile hydrolysis-based chemical destruction of the warfare agents VX, GB, and HD by alumina-supported fluoride reagents, J. Org. Chem. 74 (2009) 329–338.
[12] Y.S. Simanenko, V.A. Savelova, T.M. Prokop'eva, V.A. Mikhailov, M.K. Turovskaya, E.A. Karpichev, A.F. Popov, N.D. Gillitt, C.A. Bunton, Bis(dialkylamide)hydrogen dibromobromate precursors of hypobromite ion in reactions with nerve and blister agent simulants, J. Org. Chem. 69 (2004) 9238–9240, references therein.
[13] A.V. Vorontsov, Y.-C. Chen, P.G. Smirniotis, Photocatalytic oxidation of VX simulant 2-(butylamino)ethanethiol, J. Hazard. Mater. B 113 (2004) 89–95, references therein.
[14] A. Michalkova, L. Gorb, M. Ilchenko, O.A. Zhikol, O.V. Shishkin, J. Leszczynski, Adsorption of sarin and soman on dickite: an ab initio ONIOM study, J. Phys. Chem. B 108 (2004) 1918–1930.
[15] C.M. Hill, W.-S. Li, J.B. Thoden, H.M. Holden, F.M. Raushel, Enhanced degradation of chemical warfare agents through molecular engineering of the phosphotriesterase active site, J. Am. Chem. Soc. 125 (2003) 8990–8991.
[16] G. Amitai, R. Adani, M. Hershkovitz, P. Bel, I. Rabinovitz, H. Meshulam, Degradation of VX and sulfur mustard by enzymatic haloperoxidation, J. Appl. Toxicol. 23 (2003) 225–233.
[17] J.J. Kiddle, S.P. Mezyk, Reductive destruction of chemical warfare agent simulants in water, J. Phys. Chem. B 108 (2004) 9568–9570.
[18] N.B. Munro, K.R. Ambrose, A.P. Watson, Toxicity of the organophosphate chemical warfare agents GA, GB, and VX: implications for public protection, Environ. Health Perspect. 102 (1994) 18–37.
[19] F. Zheng, C.G. Zhan, R.L. Ornstein, Theoretical studies of reaction pathways and energy barriers for alkaline hydrolysis of phosphotriesterase substrates paraoxon and related toxic phosphofluoridate nerve agents, J. Chem. Soc., Perkin Trans. 2 (2001) 2355–2363.
[20] S. Bhattacharya, V.P. Kumar, Effect of heteroatom insertion at the side chain of 5-alkyl-1*H*-tetrazoles on their properties as catalysts for ester hydrolysis at neutral pH, J. Org. Chem. 70 (2005) 9677–9685.
[21] R.A. Moss, S. Bose, K.G. Ragunathan, N. Jayasuriya, T.J. Emge, An exceptionally reactive phosphotriester, Tetrahedron Lett. 39 (1998) 347–350.
[22] K.L. Klinkel, L.A. Kiemele, D.L. Gin, J.R. Hagadorn, Rapid phosphorus triester hydrolysis catalyzed by bimetallic tetrabenzimidazole complexes, Chem. Commun. (2006) 2919–2921.
[23] C.A. Bunton, S.J. Farber, E.J. Fendler, Hydrolysis of p-nitrophenyl diphenl phosphate, J. Org. Chem. 33 (1968) 29–33.
[24] C.A. Bunton, L. Robinson, Micellar effects upon the reaction of p-nitrophenyl diphenyl phosphate with hydroxide and fluoride ions, J. Org. Chem. 34 (1969) 773–780.
[25] S.L. Bartelt-Hunt, D.R.U. Knappe, M.A. Barlaz, Evaluation of chemical warfare agent simulants for environmental applications, Crit. Rev. Environ. Sci. Tech. 38 (2008) 112–136.
[26] T.A. Halgren, Merck molecular force field. V. Extension of MMFF94 using experimental data, additional computational data and empirical rules, J. Comput. Chem. 17 (1996) 616–641.
[27] T.A. Halgren, Merck molecular force field. III. Molecular geometries and vibrational frequencies for MMFF94, J. Comput. Chem. 17 (1996) 553–586.
[28] T.A. Halgren, Merck molecular force field. II. MMFF94 van der Waals and electrostatic parameters for intermolecular interactions, J. Comput. Chem. 17 (1996) 520–552.
[29] T.A. Halgren, Merck molecular force field. I. Basis, form, scope, parameterization, and performance of MMFF94, J. Comput. Chem. 17 (1996) 490–519.
[30] T.A. Halgren, R.B. Nachbar, Merck molecular force field. IV. Conformational energies and geometries for MMFF94, J. Comput. Chem. 17 (1996) 587–615.
[31] M. Saunders, K.N. Houk, Y.D. Wu, W.C. Still, M. Lipton, G. Chang, W.C. Guida, Conformations of cycloheptadecane. A comparison of methods for conformational searching, J. Am. Chem. Soc. 112 (1990) 1419–1427.
[32] E. Polak, G. Ribiere, Note surla convergence des methodes de directions conjuguees, Rev. Fr. Inf. Rech. Oper. 16-R1 (1969) 35–43.
[33] G. Chang, W.C. Guida, W.C. Still, An internal-coordinate Monte Carlo method for searching conformational space, J. Am. Chem. Soc. 111 (1989) 4379–4386.
[34] P.S. Shenkin, D.Q. McDonald, Cluster analysis of molecular conformations, J. Comput. Chem. 15 (1994) 899–916.
[35] S.D. Hillson, E. Smith, M. Zeldin, C.A. Parish, Cages, baskets, ladders, and tubes: conformational studies of polyhedral oligomeric silsesquioxanes, J. Phys. Chem. A 109 (2005) 8371–8378.
[36] A.D. Becke, Density-functional thermo chemistry. III. The role of exact exchange, J. Chem. Phys. 98 (1993) 5648–5652.
[37] C. Lee, W. Yang, R.G. Parr, Development of the Colle-Salvetti correlation-energy formula into a functional of the electron density, Phys. Rev. B 37 (1988) 785–789.
[38] J.M. Beck, C.M. Hadad, Hydrolysis of nerve agents by model nucleophiles: a computational study, Chem. Biol. Interact. 175 (2008) 200–203.
[39] C. González, H.B. Schlegel, Reaction path following in mass-weighted internal coordinates, J. Phys. Chem. 94 (1990) 5523–5527.
[40] C. González, H.B. Schlegel, Improved algorithms for reaction path following: higher-order implicit algorithms, J. Chem. Phys. 95 (1991) 5853–5860.
[41] C. Møller, M.S. Plesset, Note on an approximation treatment for many-electron systems, Phys. Rev. 46 (1934) 618–622.
[42] W.J. Hehre, L. Radom, P.v.R. Schleyer, J.A. Pople, Ab initio Molecular Orbital Theory, Wiley Interscience, New York, 1986.
[43] M.T. Cancès, B. Mennucci, J. Tomasi, A new integral equation formalism for the polarizable continuum model: theoretical background and applications to isotropic and anisotropic dielectrics, J. Chem. Phys. 107 (1997) 3032–3041.
[44] A.K. Rappé, C.J. Casewit, K.S. Colwell, W.A. Goddard III, W.M. Skiff, UFF, a full periodic table force field for molecular mechanics and molecular dynamics simulations, J. Am. Chem. Soc. 114 (1992) 10024–10035.
[45] M.J. Frisch, G.W. Trucks, H.B. Schlegel, G.E. Scuseria, M.A. Robb, J.R. Cheeseman, J.A. Montgomery Jr., T. Vreven, K.N. Kudin, J.C. Burant, J.M. Millam, S.S. Iyengar, J. Tomasi, V. Barone, B. Mennucci, M. Cossi, G. Scalmani, N. Rega, G.A. Petersson, H. Nakatsuji, M. Hada, M. Ehara, K. Toyota, R. Fukuda, J. Hasegawa, M. Ishida, T. Nakajima, Y. Honda, O. Kitao, H. Nakai, M. Klene, X. Li, J.E. Knox, H.P. Hratchian, J.B. Cross, V. Bakken, C. Adamo, J. Jaramillo, R. Gomperts, R.E. Stratmann, O. Yazyev, A.J. Austin, R. Cammi, C. Pomelli, J.W. Ochterski, P.Y. Ayala, K. Morokuma, G.A. Voth, P. Salvador, J.J. Dannenberg, V.G. Zakrzewski, S. Dapprich, A.D. Daniels, M.C. Strain, O. Farkas, D.K. Malick, A.D. Rabuck, K. Raghavachari, J.B. Foresman, J.V. Ortiz, Q. Cui, A.G. Baboul, S. Clifford, J. Cioslowski, B.B. Stefanov, G. Liu, A. Liashenko, P. Piskorz, I. Komaromi, R.L. Martin, D.J. Fox, T. Keith, M.A. Al-Laham, C.Y. Peng, A. Nanayakkara, M. Challacombe, P.M.W. Gill, B. Johnson, W. Chen, M.W. Wong, C. Gonzalez, J.A. Pople, Gaussian 03, Revision E.01, Gaussian, Inc., Wallingford, CT, 2004.
[46] W. Yang, R.G. Parr, Hardness, softness, and the fukui function in the electronic theory of metals and catalysis, Proc. Natl. Acad. Sci. U.S.A. 82 (1985) 6723–6726.
[47] F. De Proft, J.M.L. Martin, P. Geerlings, On the performance of density functional methods for describing atomic populations, dipole moments and infrared intensities, Chem. Phys. Lett. 250 (1996) 393–401.
[48] C. Lee, W. Yang, R.G. Parr, Phys. Rev. B 37 (1988) 785–789.
[49] T.A. Koopmans, Physica 1 (1933) 104.
[50] J.L. Gázquez, The hard and soft acids and bases principle, J. Phys. Chem. A 101 (1997) 4657–4659.
[51] L.T. Nguyen, T.N. Le, F. De Proft, A.K. Chandra, W. Langenaeker, M.T. Nguyen, P. Geerlings, Mechanism of [2 + 1] cycloadditions of hydrogen isocyanide to alkynes: molecular orbital and density functional theory study, J. Am. Chem. Soc. 121 (1999) 5992–6001.
[52] A. Ponti, DFT-based regioselectivity criteria for cycloaddition reactions, J. Phys. Chem. A 104 (2000) 8843–8846.
[53] B.J. Lynch, D.G. Truhlar, How well can hybrid density functional methods predict transition state geometries and barrier heights? J. Phys. Chem. A 105 (2001) 2936–2941.
[54] J. Baker, M. Muir, J. Andzelm, A study of some organic reactions using density functional theory, J. Chem. Phys. 102 (1995) 2063–2079.
[55] J. Purcell, A.C. Hengge, The thermodynamics of phosphate versus phosphorothioate ester hydrolysis, J. Org. Chem. 70 (2005) 8437–8442.
[56] J. Florian, A. Warshel, Phosphate ester hydrolysis in aqueous solution: associative versus dissociative mechanisms, J. Phys. Chem. B 102 (1998) 719–734.
[57] J. Šečkutė, J.L. Menke, R.J. Emnett, E.V. Patterson, C.J. Cramer, Ab initio molecular orbital, and density functional studies on the solvolysis of sarin and *O,S*-dimethyl methylphosphonothiolate, a VX-like compound, J. Org. Chem. 70 (2005) 8649–8660.
[58] E.V. Patterson, C.J. Cramer, Molecular orbital calculations on the P—S bond cleavage step in the hydroperoxidolysis of nerve agent VX, J. Phys. Org. Chem. 11 (1998) 232–240.
[59] K.A. Daniel, L.A. Kopff, E.V. Patterson, Computational studies on the solvolysis of the chemical warfare agent VX, J. Phys. Org. Chem. 21 (2008) 321–328.
[60] J.L. Menke, E.V. Patterson, Quantum mechanical calculations on the reaction of ethoxide anion with *O,S*-dimethyl methylphosphonothiolate, J. Mol. Struct. THEOCHEM 811 (2007) 281–291.
[61] M.A.S. Khan, M.K. Kesharwani, T. Bandyopadhyay, B. Ganguly, Solvolysis of chemical warfare agent VX is more efficient with hydroxylamine anion: a computational study, J. Mol. Graph. Model. 28 (2009) 177–182.
[62] M.A.S. Khan, M.K. Kesharwani, T. Bandyopadhyay, B. Ganguly, Remarkable effect of hydroxylamine anion towards the solvolysis of sarin: a DFT study, J. Mol. Struct. THEOCHEM 944 (2010) 132–136.
[63] M.K. Kesharwani, M.A.S. Khan, T. Bandyopadhyay, B. Ganguly, Solvolysis process of organophosphorus compound *P*-[2-(dimethylamino)ethyl]-*NN*-dimethylphosphonamidic fluoride with simple and α-nucleophiles: a DFT study, Theor. Chem. Acc. 127 (2010) 39–47.
[64] K.K. Ghosh, D. Sinha, M.L. Satnami, D.K. Dubey, P. Rodriguez-Dafonte, G.L. Mundhara, Nucleophilic dephosphorylation of *p*-nitrophenyl diphenyl phosphate in cationic micellar media, Langmuir 21 (2005) 8664–8669.

[65] S.H. Gellman, R. Petter, R. Breslow, Catalytic hydrolysis of a phosphate triester by tetracoordinated zinc complexes, J. Am. Chem. Soc. 108 (1986) 2388–2394.
[66] H. Chermette, Chemical reactivity indexes in density functional theory, J. Comput. Chem. 20 (1999) 129–154.
[67] P.K. Chattaraj, S. Nath, B. Maiti, in: J. Tollenaere, P. Bultinck, H.D. Winter, W. Langenaeker (Eds.), Reactivity Descriptors. In Computational Medicinal Chemistry and Drug Discovery, Marcel Dekker, New York, 2003, pp. 295–322.
[68] J. Korchowiec, T. Uchimuaru, Mechanism of addition of fluoromethyl radicals to fluoroethylenes, J. Phys. Chem. A 102 (1998) 6682–6689.